Acta Mechanica 101, 45–57 (1993)

ACTA MECHANICA

A local solution method for shock boundary-layer interaction on a swept wing

P.-Ch. Nellner and **J. Zierep,** Karlsruhe, Federal Republic of Germany

(Received May 5, 1992)

Summary. The paper describes a local solution method for the calculation of the interaction between a weak shock front and a turbulent boundary layer on a swept wing. A multiple-deck approach allows the simplification of the governing equations according to the physical character of each deck. The mathematical model is based upon small-perturbation theory. The final boundary-layer solution is given by an iterative coupling of the solutions for each domain. The results are compared with experiments and with other theoretical solutions.

1 Introduction

The aerodynamic performance of supercritical wings at transonic speeds is strongly influenced by shock boundary-layer interactions. The flow is characterized by a shock wave standing on the upper side of the wing. The adverse pressure gradient can induce boundary-layer separation, which may increase drag and reduce lift. A comprehensive review of the interaction problem is given by Delery and Marvin [1] and by Stanewsky [2].

In 1976 Bohning and Zierep [3] developed a local solution method for the two-dimensional interaction problem. This method could be adapted to the self-acting ventilation flow over a perforated wall induced by the pressure rise in the shock region [4] and has been inserted into a zonal solution procedure for the description of flows past airfoils and through channels without/with passive control device [5]. Due to the good agreement between theory and experiment [6], [7], the local solution method has been extended to the interactive flow over an infinite swept wing.

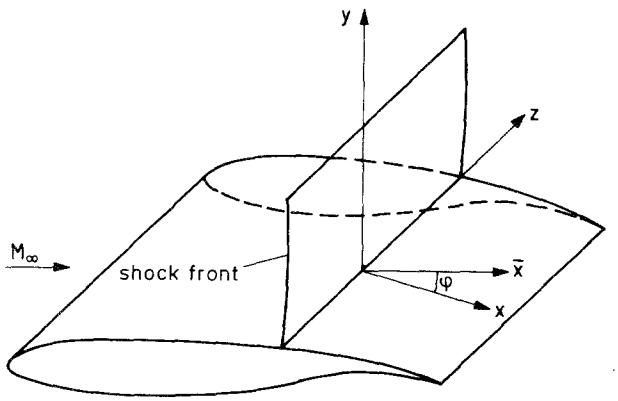

Fig. 1. Swept wing with shock front

A swept back wing is comprised of several two-dimensional airfoil profiles. The profiles can be thought of as being aligned side by side and shifted backward. At the tip of the wing and its root no simplification is possible with regard to the general three-dimensional flow. But in the middle part the derivatives with respect to the spanwise z-direction can be neglected. The infinite swept wing is thus a model for the flow field in the midspan of a large aspect ratio wing.

Figure 1 shows an infinite swept wing with shock front. The leading edge, the shock trace (z-axis), and the trailing edge have the same direction. The angle φ between the freestream direction ($\bar{x}$-axis) and the direction normal to the shock front (x-axis) is the sweep angle. The freestream velocity can be splitted up into a component in x-direction and a component in z-direction. In the inviscid outer flow the z-component is constant (superposed tangential velocity). However, it is not possible to reduce the system of momentum equations to an independent two-dimensional flow in chordwise direction and a dependent spanwise flow, because in the boundary layer the change of density due to the tangential velocity depends on the distance to the wall.

2 Multiple-deck approach and mathematical model

The interactive flow is taken to be a local problem and therefore the velocity distribution at the boundary-layer edge is required, which yields the pressure distribution p_δ. The pressure gradient normal to the shock at the boundary-layer edge is large, even for weak shocks. Because this gradient is softened towards the wall, the classical boundary-layer assumption $\partial p/\partial y = 0$ is not valid in the interaction region. The basic idea of the model for the flow field is to divide the interaction region into three decks: an inviscid outer flow, a shear layer, and a wall layer (Fig. 2). The estimation of the orders of magnitude for high Reynolds numbers [8] shows that in the outer part of the boundary layer the pressure gradient normal to the wall has to be taken into account, but the friction terms can be omitted. In the inner part the pressure distribution is given by the shear-layer flow, while the main friction terms are preserved.

The thermodynamic quantities pressure p, temperature T, and density ϱ are normalized by their critical values p^*, ϱ^*, T^*. The velocities u, v, and w are referred to the critical velocity of sound $c^* = \sqrt{\gamma p^*/\varrho^*}$. Thus the absolute value of the modulus of the velocity vector is the critical Mach number. The boundary-layer thickness δ is chosen as the characteristic length for the coordinates. Then the Reynolds number becomes $\mathrm{Re} = c^*\delta\varrho^*/\mu$.

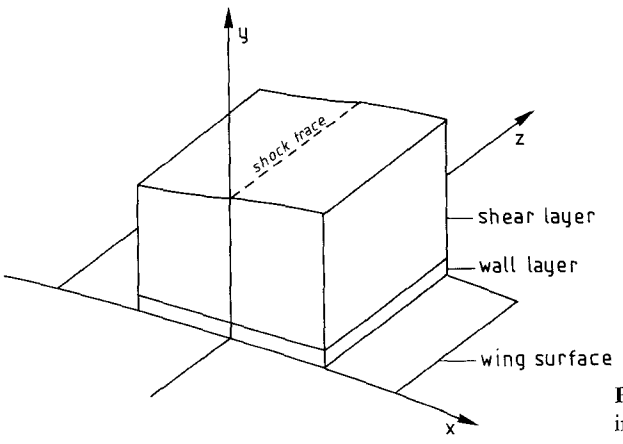

Fig. 2. Model for the flow field in the interaction region

Considering a weak shock wave and a slightly curved body surface, it is obvious to use a perturbation technique. Because former studies of the second-order theory for the two-dimensional case have shown that the solution differs hardly from the first-order solution, in the present paper all unknown variables are replaced by the quantities for the basic flow (subscript 0) and for the first-order perturbations (subscript 1):

$$p(x, y) = 1 + p_1(x, y) \tag{1}$$

$$T(x, y) = T_0(y) + T_1(x, y) \tag{2}$$

$$\varrho(x, y) = \varrho_0(y) + \varrho_1(x, y) \tag{3}$$

$$u(x, y) = u_0(y) + u_1(x, y) \tag{4}$$

$$v(x, y) = v_1(x, y) \tag{5}$$

$$w(x, y) = w_0(y) + w_1(x, y). \tag{6}$$

Due to the slight curvature of the flow field, it is assumed for the basic flow that the derivatives with respect to the x-direction can be neglected. The basic velocity profile is split up into the components $u_0 = \cos \psi M_0{}^*$, $v_0 = 0$, and $w_0 = \sin \psi M_0{}^*$, where ψ is the angle of the incoming flow to the x-axis. The critical Mach number of the basic flow can be converted to the local Mach number M_0:

$$M_0 = \frac{1}{\sqrt{\dfrac{\gamma+1}{2} - \dfrac{\gamma-1}{2} M_0{}^{*2}}} M_0{}^* = \sqrt{\varrho_0}\, M_0{}^*. \tag{7}$$

The basic pressure $p_0 = 1$ in the boundary layer is constant. Therefore it is possible to represent the turbulent velocity distribution by a power law [9]:

$$M_0{}^* = y^\alpha, \qquad M_0 = y^\beta. \tag{8}$$

In the wall layer, similiar to the laminar sublayer, the basic velocity distribution is a linear function.

The basic flow with the constant critical pressure and the Mach number $M_0{}^* = M_0 = 1$ at the boundary-layer edge represents the turbulent boundary layer on a flat plate, whereas the added disturbance variables describe the influence of the shock front and of the wall curvature.

Taking into account (1)–(6), the perturbation equations of continuity, energy, and state become

$$\varrho_0 \frac{\partial u_1}{\partial x} + u_0 \frac{\partial \varrho_1}{\partial x} + \frac{\partial}{\partial y}(\varrho_0 v_1) = 0 \tag{9}$$

$$T_1 = -(\gamma - 1)(u_0 u_1 + w_0 w_1) \tag{10}$$

$$p_1 = \varrho_0 T_1 + \varrho_1 T_0. \tag{11}$$

With respect to the momentum equations we have to distinguish between the outer and the inner part of the boundary layer. If the shear layer is considered, we obtain

$$\varrho_0 u_0 \frac{\partial u_1}{\partial x} + \varrho_0 v_1 \frac{du_0}{dy} = -\frac{1}{\gamma} \frac{\partial p_1}{\partial x} \tag{12}$$

$$\varrho_0 u_0 \frac{\partial v_1}{\partial x} = -\frac{1}{\gamma} \frac{\partial p_1}{\partial y} \tag{13}$$

$$\varrho_0 u_0 \frac{\partial w_1}{\partial x} + \varrho_0 v_1 \frac{dw_0}{dy} = 0. \tag{14}$$

Adjacent to the wall the momentum equations are given by

$$\varrho_0 u_0 \frac{\partial u_1}{\partial x} + \varrho_0 v_1 \frac{du_0}{dy} = -\frac{1}{\gamma} \frac{\partial p_1}{\partial x} + \frac{1}{\mathrm{Re}} \frac{\partial^2 u_1}{\partial y^2} \tag{15}$$

$$\frac{\partial p_1}{\partial y} = 0 \tag{16}$$

$$\varrho_0 u_0 \frac{\partial w_1}{\partial x} + \varrho_0 v_1 \frac{dw_0}{dy} = \frac{1}{\mathrm{Re}} \frac{\partial^2 w_1}{\partial y^2}. \tag{17}$$

3 Local solution

3.1 Shear layer

The solution for the outer boundary layer is obtained this way: Replacing T_1 in (11) by (10) allows to eliminate ϱ_1 in the continuity equation (9). Then the derivatives of u_1 and w_1 from (12), (14) can be applied. Now there are two equations under consideration: the continuity and the second momentum equation. The only two unknown variables here are p_1 and v_1. Equation (13) can be satisfied by

$$p_1 = -\gamma \Phi_x \tag{18}$$

$$v_1 = \frac{1}{\varrho_0 u_0} \Phi_y. \tag{19}$$

Using these representations, the system of the perturbation equations (9)–(14) is reduced to one equation

$$(1 - \varrho_0 {u_0}^2)\, \Phi_{xx} + \Phi_{yy} - \frac{2}{\sqrt{\varrho_0}\, u_0} \frac{d}{dy} \left(\sqrt{\varrho_0}\, u_0\right) \Phi_y = 0 \tag{20}$$

for the unknown variable Φ. Due to (18), (19), boundary conditions in terms of p_1 and v_1 are needed. At the edge of the boundary layer $p_1(x, 1)$ is given by the outer flow. If a parallel stream adjacent to the wall is considered, v_1 vanishes at the inner boundary-layer edge. At the beginning and at the end of the interaction region ($x \leqq x_b$, $x \geqq x_e$) we assume $\partial/\partial x \approx 0$. Hence, the boundary conditions related to Φ are

$$\Phi_x(x, 1) = -\frac{1}{\gamma} p_1(x, 1) \tag{21}$$

$$\Phi_y(x, y_\mu) = 0 \tag{22}$$

$$\Phi_y(x_b, y) = \Phi_y(x_e, y) = 0. \tag{23}$$

The problem (20)–(23) can be solved using the separation method. The function Φ is represented by the sum of a function f_n depending on y times a function g_n, depending on x:

$$\Phi(x, y) = \sum_{n=1}^{\infty} f_n(y)\, g_n(x) - \frac{1}{\gamma} \int_{x_b}^{x} p_1(\xi, 1)\, d\xi. \tag{24}$$

The second term in (24) is utilized to obtain homogeneous boundary conditions for the functions f_n. Now Eq. (20) divides into two ordinary equations coupled by the separation parameter λ_n.

With respect to (7), (8) the Sturm-Liouville problem in y-direction can be written as

$$\frac{d}{dy}\left(\frac{1}{y^{2\beta}} \frac{df_n}{dy}\right) + \lambda_n \left(\frac{1 - \cos^2 \psi y^{2\beta}}{y^{2\beta}}\right) f_n = 0 \tag{25}$$

$$f_n(1) = 0 \tag{26}$$

$$\frac{df_n(y_\mu)}{dy} = 0. \tag{27}$$

The integration of the eigenvalue problem (25)–(27)

$$\int_{y_\mu}^{1} \frac{1 - \cos^2 \psi y^{2\beta}}{y^{2\beta}} f_n\, dy = -\frac{1}{\lambda_n} \frac{df_n(1)}{dy} \tag{28}$$

simplifies the representation of the coefficients d_n in the equation of oscillation (44) below. To get the solution of the eigenvalue problem, at first, the expression

$$1 - \cos^2 \psi y^{2\beta} \approx a y^{\varkappa - 2} - b y^{2(\varkappa - 1)} \tag{29}$$

is replaced. For the two-dimensional case we have

$$a_{2D} = b_{2D} = 4\beta(\beta + 1)^{-\frac{\beta+1}{\beta}} \tag{30}$$

$$\varkappa_{2D} = 2\beta \frac{\ln 2}{\ln (2\beta + 1)} \tag{31}$$

and in case of $\psi \neq 0$

$$H = \frac{2 \sin^2 \psi - a_{2D} \varkappa_{2D} \cos^2 \psi}{4 \sin^2 \psi - 3 a_{2D} \varkappa_{2D}^2 \cos^2 \psi} \tag{32}$$

$$a = 2 \sin^2 \psi - \frac{3}{2} H + \frac{1}{2} \sqrt{9H^2 - 8H \sin^2 \psi} \tag{33}$$

$$b = a - \sin^2 \psi \tag{34}$$

$$\varkappa = \frac{2 \sin^2 \psi - a_{2D} \varkappa_{2D} \cos^2 \psi}{a - 2b}. \tag{35}$$

Then the coordinate y and the eigenfunctions f_n are transformed:

$$\eta = \frac{2\sqrt{b\lambda_n}}{\gamma} y^{\varkappa} = \sigma_n y^{\varkappa} \tag{36}$$

$$h_n = f_n \exp\left(\frac{1}{2}\eta\right) \eta^{-\frac{2\beta+1}{\varkappa}}. \tag{37}$$

With the abbreviations

$$\omega = \frac{2\beta + 1 + \varkappa}{\varkappa} \tag{38}$$

$$q_n = \frac{\omega}{2} - \frac{\sigma_n}{4}\frac{a}{b}, \tag{39}$$

Eq. (25) changes into

$$\eta \frac{d^2 h_n}{d\eta^2} + (\omega - \eta)\frac{dh_n}{d\eta} - q_n h_n = 0. \tag{40}$$

This type of differential equation is solved by confluent hypergeometric functions [10], in a general representation given by

$$M(a, b, x) = 1 + \sum_{n=1}^{\infty} \frac{a(a+1)\ldots(a+n-1)}{b(b+1)\ldots(b+n-1)} \frac{x^n}{n!}. \tag{41}$$

The solution of (40) is

$$h_n(\eta) = A \cdot M(q_n, \omega, \eta) + \eta^{1-\omega} B \cdot M(1 + q_n - \omega, 2 - \omega, \eta). \tag{42}$$

Recalling the transformations (36), (37), the constants A, B can be determined with the conditions (26), (27). The solution of the eigenvalue problem becomes

$$f_n(y) = \exp\left(-\frac{\sigma_n}{2} y^{\varkappa}\right) N_n \{ y^{2\beta+1} M(1 + q_n - \omega, 2 - \omega, \sigma_n)\, M(q_n, \omega, \sigma_n y^{\varkappa}) - M(1 + q_n - \omega, 2 - \omega, \sigma_n y^{\varkappa})\, M(q_n, \omega, \sigma_n)\}. \tag{43}$$

The parameter σ_n is obtained from the eigenvalue determinant, N_n follows from the orthogonality relations.

The equation of oscillation in x-direction and the associated boundary conditions are

$$\frac{d^2 g_n}{dx^2} - \lambda_n g_n = d_n(x) \tag{44}$$

$$g_n(x_b) = g_n(x_e) = 0. \tag{45}$$

With respect to (28) the coefficients d_n can be written as

$$d_n(x) = \frac{1}{\gamma}\frac{dp_1(x,1)}{dx} \int_{y_\mu}^{1} \frac{1 - \cos^2 \psi y^{2\beta}}{y^{2\beta}} f_n \, dy = -\frac{1}{\gamma}\frac{dp_1(x,1)}{dx}\frac{1}{\lambda_n}\frac{df_n(1)}{dy}. \tag{46}$$

The solution of (44), (45) is given by

$$g_n(x) = \frac{1}{\sqrt{\lambda_n}} \left\{ \int_{x_b}^{x} d_n(\xi) \sinh \sqrt{\lambda_n}(x-\xi)\, d\xi - \frac{\sinh \sqrt{\lambda_n}(x-x_b)}{\sinh \sqrt{\lambda_n}(x_e-x_b)} \int_{x_b}^{x_e} d_n(x) \sinh \sqrt{\lambda_n}(x_e-x)\, dx \right\}. \tag{47}$$

With (43), (47) the function Φ follows from (24), and with the derivatives (18), (19) we get the disturbances p_1 and v_1. Integration of (12), (14) and adaption to the incoming flow yield

$$u_1(x, y) = -\frac{p_1(x, y) - p_1(x_b, y)}{\gamma \varrho_0 u_0} - \frac{1}{u_0} \frac{du_0}{dy} \int_{x_b}^{x} v_1(\xi, y)\, d\xi + u_1(x_b, y) \tag{48}$$

$$w_1(x, y) = -\frac{1}{u_0} \frac{dw_0}{dy} \int_{x_b}^{x} v_1(\xi, y)\, d\xi + w_1(x_b, y). \tag{49}$$

Now the disturbance of the temperature and of the density can be obtained from (10), (11). Adding the quantities of the basic flow, all variables of the flow field in the outer boundary layer are given.

3.2 Wall layer

Because the solutions of the outer and the inner boundary layer depend on the thickness of the wall layer, the final boundary-layer solution is given by an implicit coupling of the outer boundary layer with the inner one. Varying the thickness y_μ of the wall layer, y_μ can be determined by the vanishing gradient of the wall-shear stress in x-direction [6]. In comparison with the overall boundary layer, the wall layer is very thin (order of magnitude: $y_\mu/\delta \sim 10^{-2}$).

Adjacent to the adiabatic wall we assume for the temperature gradient $\partial T/\partial x \approx 0$. To solve the wall-layer problem, the momentum equations (15), (17) are differentiated with respect to y. Combined with (9) merely ϱ_1 needs to be eliminated. This yields two equations for the disturbances u_1 and w_1.

For u_1 we get

$$\frac{\partial^3 u_1}{\partial y^3} - \varrho_0 u_0 \frac{\partial^2 u_1}{\partial x\, \partial y} = -\varrho_0 u_0 \frac{dp_1}{dx} \frac{du_0}{dy}. \tag{50}$$

At the inner boundary-layer edge u_1 is given by the shear-layer flow. At the wall u_1 has to vanish and from (15) follows

$$\frac{\partial^2 u_1}{\partial y^2} = \frac{\mathrm{Re}}{\gamma} \frac{dp_1}{dx} = u_{yy,W}. \tag{51}$$

A particular solution (adapted to the incoming flow) of Eq. (50) is

$$u_{1p} = \{p_1(x) - p_1(x_b)\}\, u_0(y) + u_1(x_b, y). \tag{52}$$

Provided the homogeneous solution is of the same structure

$$u_{1h} = \{p_1(x) - p_1(x_b)\}\, f(y) \tag{53}$$

we have to solve

$$\frac{d^3f}{dy^3} - \underbrace{\frac{1}{p_1(x) - p_1(x_b)} \frac{dp_1}{dx}}_{=G^2} \varrho_0 \frac{du_0}{dy} y \frac{df}{dy} = 0. \tag{54}$$

The transformations

$$\frac{df}{dy} = y^{1/2} h \tag{55}$$

$$\eta = \frac{2}{3} G y^{3/2} \tag{56}$$

lead to

$$\frac{d^2h}{d\eta^2} + \frac{1}{\eta} \frac{dh}{d\eta} - \left(1 + \frac{1}{9\eta^2}\right) h = 0. \tag{57}$$

The general solution [10] is given by

$$h(\eta) = AI_{-1/3}(\eta) + BI_{1/3}(\eta) \tag{58}$$

$$I_\nu(\eta) = \sum_{k=0}^{\infty} \frac{\left(\frac{1}{2}\eta\right)^{2k+\nu}}{k!\,\Gamma(\nu + k + 1)} \tag{59}$$

where the functions I_ν are modified Bessel functions. Γ means Euler's Gamma function. Summing up the particular and the homogeneous solution, the constants of integration A, B are obtained from the boundary conditions. We get

$$u_1 = u_1(x_b, y) + (p_1 - p_1(x_b)) \left\{ u_0 + \int_0^y \zeta^{1/2} (AI_{-1/3} + BI_{1/3})\, d\zeta \right\} \tag{60}$$

with

$$B = \frac{u_{yy,w}}{p_1 - p_1(x_b)} \frac{\Gamma\left(\frac{1}{3}\right)}{G} \left(\frac{G}{3}\right)^{2/3} \tag{61}$$

$$A = \left\{ \frac{u_1(x, y_\mu) - u_1(x_b, y_\mu)}{p_1 - p_1(x_b)} - u_0(y_\mu) - B \int_0^{y_\mu} y^{1/2} I_{1/3}\, dy \right\} \frac{1}{\int_0^{y_\mu} y^{1/2} I_{-1/3}\, dy}. \tag{62}$$

The same procedure applied to w_1 yields

$$\frac{\partial^3 w_1}{\partial y^3} - \varrho_0 u_0 \frac{\partial^2 w_1}{\partial x\, \partial y} = -\varrho_0 u_0 \frac{dp_1}{dx} \frac{du_0}{dy} \tag{63}$$

$$w_{yy,w} = 0 \tag{64}$$

$$w_1 = w_1(x_b, y) + (p_1 - p_1(x_b)) \left\{ w_0 + C \int_0^y \zeta^{1/2} I_{-1/3}\, d\zeta \right\} \tag{65}$$

$$C = \frac{-w_0(y_\mu)}{\int_0^{y_\mu} y^{1/2} I_{-1/3}\, dy}. \tag{66}$$

Again the disturbances T_1 and ϱ_1 follow from (10), (11), and with the quantities of the basic flow all variables of the inner boundary layer can be calculated.

3.3 Coupling with the inviscid outer flow

To apply the present boundary-layer method, the required local input data are derived this way: The incoming velocity profile is represented by the normal and the tangential component of the critical Mach number M^* at the boundary-layer edge and by the incompressible shape factor H_i (ratio of incompressible displacement thickness and momentum thickness). In a first step, a pressure jump due to the Prandtl-relation for oblique shocks is considered. This "pressure distribution" is the boundary condition for the shear-layer problem, whose solution provides the distribution of the velocity v normal to the wall. In the next step, v is the boundary condition for the inviscid outer flow. The outer flow can be reduced to the two-dimensional case, because in this domain the spanwise velocity depends neither on x nor on y; the chordwise velocity depends on the local radius R of the wing surface normal to the shock [6], [11]. This leads to a new pressure distribution at the boundary-layer edge. Thereupon the shear-layer problem is solved again and, finally, coupled with the wall-layer problem.

4 Results

Figure 3 shows the pressure distribution at the boundary-layer edge (p_δ) and at the wall (p_W). The shock position is at $x = 0$. The dashed lines refer to the pressure jump in the outer flow due to the Prandtl-relation (starting solution). At the wall the pressure rise is just the same, but it is a more gradual one. About six boundary-layer thicknesses are needed to reach the downstream value of the shock wave. The full lines show the pressure distribution due to the interaction with the outer flow (final solution). Even ahead of the shock front p_δ increases, and behind the shock front the post-shock expansion can be seen; the latter was first mentioned by Ackeret, Feldmann, and Rott [12]. Accordingly, the pressure jump itself is smaller and the pressure rise at the wall is weaker.

The pressure rise is responsible for a possible boundary-layer separation. As derived by Stanewsky [2] and according to our results, the interactive flow normal to the shock front, the associated upstream influence, and the separation onset are essentially independent of a superposed tangential velocity. If the spanwise component becomes larger, the level of the pressure distribution is decreasing, but the pressure gradient is much the same and the change of density seems to be not strong enough to cause a distinct influence.

Mignosi, Dor, and Seraudie [13] have published an experimental study of the separation conditions given by the local Mach number M and the incompressible shape factor H_i upstream of the shock. Following this representation, the calculated separation onset for the two-

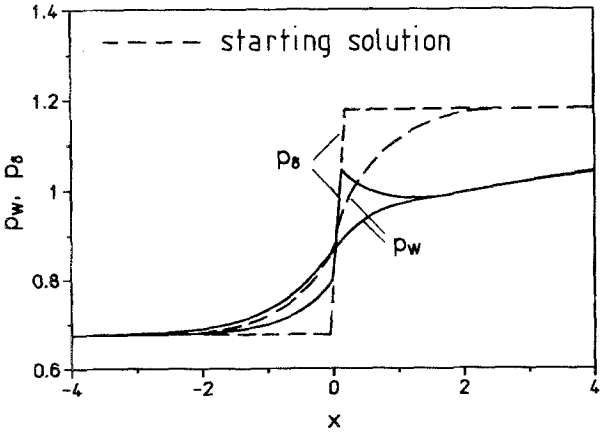

Fig. 3. Pressure distribution at the boundary-layer edge p_δ and at the wall p_W. $M^* = 1.24$, $\psi = 14$ deg, $H_i = 1.30$, $R/\delta = 400$

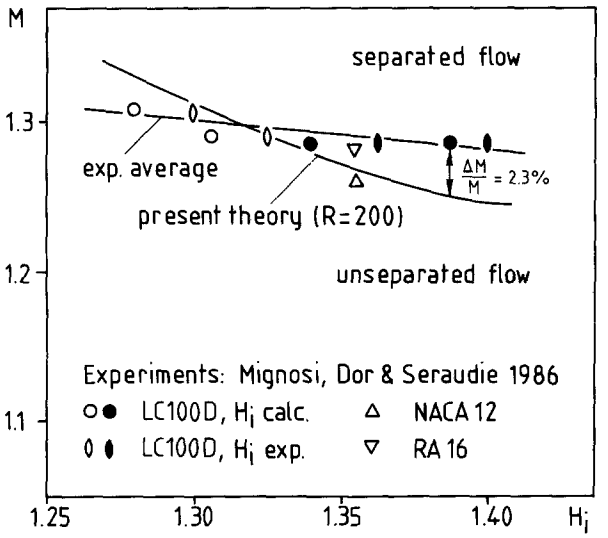

Fig. 4. Comparison of the 2D-separation condition. Experimental results [13] and present theory (R in units of δ)

dimensional case can be compared with the experimental results (Fig. 4). An increase of the shape factor leads to a lower incipient-separation Mach number. The experiments indicate a weaker influence of the shape factor than the present theory. The difference is caused by the dissimiliar local curvature of the investigated airfoil profiles, by the two methods for the determination of the shape factor, and by the different obstruction of the wind-tunnel test section due to the various size of the airfoil profiles. However, the difference between the theoretical limit for shock-induced separation and the experimental average is small.

Considering the numerical simulations of the DFVLR-F5 complete wing experiment [14], a qualitative comparison with the present results was carried out for the midspan region. Most of the results show chordwise regions of separated flow along the midspan. The calculated skin friction line patterns there correspond to the direction of the flow in Fig. 5. The arrows show the flow direction in the xz-plane close to the wall. The limiting streamlines converge into the separation line immediately ahead of the shock front. Behind the shock the flow turns back. Due to the slight curvature of the wall, the post-shock expansion is weak and, therefore, the interactive flow does not reattach.

The application of the present local solution method to a defined flow case allows a quantitative comparison with other theoretical results in the shock region. The incoming

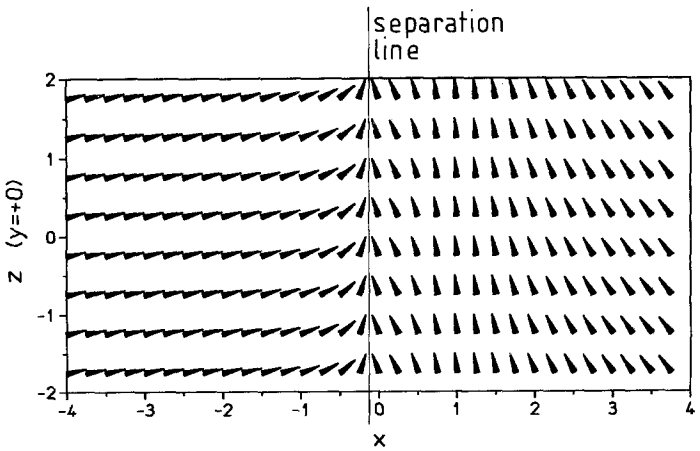

Fig. 5. Direction of the streamlines close to the surface. $M^* = 1.30$, $\psi = 14$ deg, $H_i = 1.36$, $R/\delta = 600$

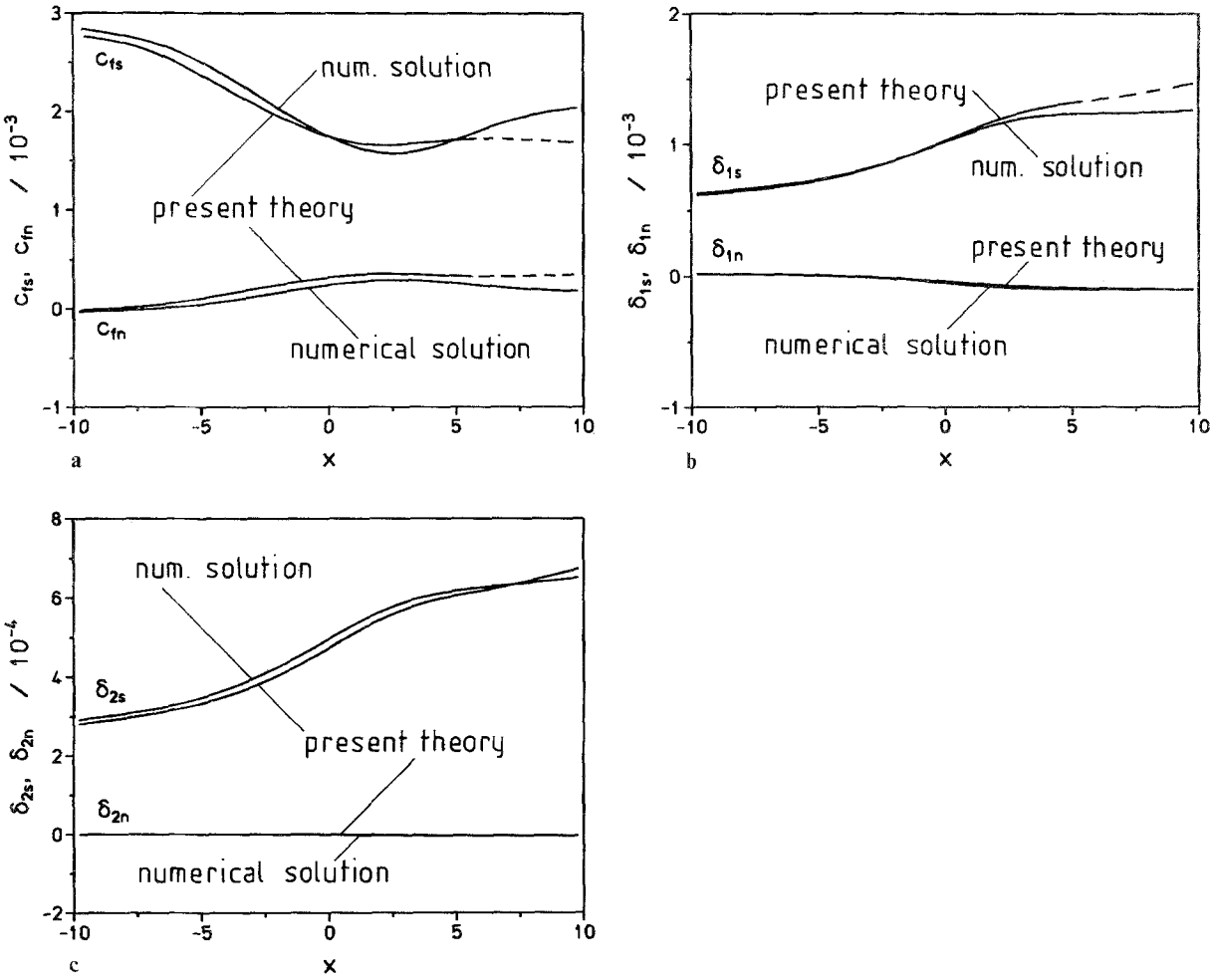

Fig. 6. Comparison with a boundary-layer calculation. Numerical method (Deutsche Airbus) and present local solution method. NACA 0012: incl. angle 1.7 deg, $\varphi = 30$ deg, $M_\infty = 0.8$, $\mathrm{Re}_\infty = 9 \cdot 10^6$; **a** skin-friction coefficients c_{fs}, c_{fn} **b** displacement thicknesses δ_{1s}, δ_{1n} **c** momentum thicknesses δ_{2s}, δ_{2n}

velocity profile and the velocity distribution at the boundary-layer edge are taken from a boundary-layer calculation for the airfoil profile NACA 0012 with a sweep angle of 30 deg and an inclination angle of 1.7 deg. The freestream conditions are $M_\infty = 0.8$ and $\mathrm{Re}_\infty = 9 \cdot 10^6$. Figure 6 ascertains the proficiency of the local method by the comparison of the skin-friction coefficient c_f, the displacement thickness δ_1, and the momentum thickness δ_2 with the numerical solution. The thicknesses are normalized by the length of the airfoil profile. All quantities are taken in the direction of the external streamline (index s) and the direction normal to it (index n). Behind the interaction region ($x > 5$) the local solution is no longer valid. Taking into account that entirely different methods are used, the agreement is remarkable.

5 Concluding remarks and outlook

The local solution method for the two-dimensional interaction between a weak shock and a turbulent boundary layer has been extended to the interactive flow over a swept wing. The comparison with experimental data and other theoretical results shows a good agreement.

Numerical calculations could profit by the present local method which benefits the resolution of the sharp gradients at the shock front. If required, a second-order solution can be derived. The first-order and the second-order solution have nearly the same structure. The coefficients d_n in the equation of oscillation (44) show additional terms, whereas the eigenvalue problem (25) does not change. A second-order solution for the wall layer can be derived, too.

A further application of the present method could be the investigation of the influence of a passive control device. An involved passive control device aims at weakening the shock strength and at delaying shock-induced separation. The pressure rise at the perforated wall causes blowing upstream of the shock and suction downstream of it. For this case, the boundary conditions for the function Φ and the inner solution depend on the distribution of the velocity component v. In comparison with the flow over a solid surface, the velocity profiles are less bulgy in the region in front of the shock and more bulgy in the region behind it. This can cause the undesired effect that the boundary layer separates even in a larger distance ahead of the shock than in the case of a solid surface. The local method adapted to swept wings with passive control device could be expedient to investigate such effects.

Acknowledgement

The authors wish to thank P. Thiede (Deutsche Airbus, Bremen, Federal Republic of Germany) for providing the numerical results.

References

[1] Délery, J., Marvin, J. G.: Shock-wave boundary layer interactions. AGARD-AG 280, 1986.
[2] Stanewsky, E.: Shock boundary layer interaction. In: Boundary layer simulation and control in wind tunnels. AGARD AR-224, pp. 271–305, 1988.
[3] Bohning, R., Zierep, J.: Der senkrechte Verdichtungsstoß an der gekrümmten Wand unter Berücksichtigung der Reibung. ZAMP **27**, 225–240 (1976).
[4] Bohning, R., Jungbluth, H.: Turbulent shock-boundary-layer interaction with control. Theory and experiment. In: Symposium Transsonicum III (Zierep, J., Oertel, H., eds.). IUTAM Symposium Göttingen, Germany 1988. Berlin Heidelberg New York Tokyo: Springer 1989.
[5] Breitling, Th.: Berechnung transsonischer, reibungsbehafteter Kanal- und Profilströmungen mit passiver Beeinflussung. Dissertation, Universität Karlsruhe 1989.
[6] Bohning, R.: Die Wechselwirkung eines senkrechten Verdichtungsstoßes mit einer turbulenten Grenzschicht an einer gekrümmten Wand. Habilitation, Universität Karlsruhe 1982.
[7] Braun, W.: Experimentelle Untersuchung der turbulenten Stoß-Grenzschicht-Wechselwirkung mit passiver Beeinflussung. Dissertation, Universität Karlsruhe 1990.
[8] Nellner, P.-Ch.: Stoß-Grenzschicht-Interferenz am schiebenden Flügel. Dissertation, Universität Karlsruhe 1991.
[9] Walz, A.: Boundary layers of flow and temperature. Cambridge/Mass. London: MIT Press 1969.
[10] Abramowitz, M., Stegun, I. A. (eds.): Pocketbook of mathematical functions. Thun Frankfurt/M.: Deutsch 1984.
[11] Oswatitsch, K., Zierep, J.: Das Problem des senkrechten Stoßes an der gekrümmten Wand. ZAMM **40**, T143–T144 (1960).
[12] Ackeret, J., Feldmann, F., Rott, N.: Investigation of compression shocks and boundary-layers in gases moving at high speed. NACA TM-1113.

[13] Mignosi, A., Dor, J. B., Seraudie, A.: Experimental study of the boundary-layer separation conditions through a shock-wave on airfoil and swept wing. In: IUTAM Symposium Turbulent Shear-Layer/Shock-Wave-Interactions Palaiseau, France 1985 (Délery, J., ed.). Berlin Heidelberg New York Tokyo: Springer 1986.

[14] Kordulla, W.: Numerical simulation of the transonic DFVLR-F5 wing experiment. Notes on numerical fluid mechanics, vol. 22. Braunschweig Wiesbaden: Vieweg 1988.

Authors' address: Dr.-Ing. P.-Ch. Nellner and Prof. Dr.-Ing. Dr. techn. E. h. J. Zierep, Institut für Strömungslehre und Strömungsmaschinen, Universität Karlsruhe, Kaiserstrasse 12, D-76131 Karlsruhe, Federal Republic of Germany